ELSEVIER

Journal of African Earth Sciences 34 (2002) 137–155

Journal of African Earth Sciences

www.elsevier.com/locate/jafrearsci

Neoproterozoic tectonothermal evolution of the Central Eastern Desert, Egypt: a slow velocity tectonic process of core complex exhumation

Harald Fritz [a,*], David R. Dallmeyer [b], Eckart Wallbrecher [a], Jürgen Loizenbauer [a], Georg Hoinkes [c], Peter Neumayr [d], Ali A. Khudeir [e]

[a] *Department of Geology and Palaeontology, Karl-Franzens-University Graz, Heinrichstrasse 26, A-8010 Graz, Austria*
[b] *Department of Geology, University of Georgia, Athens, GA 30602, USA*
[c] *Department of Mineralogy and Petrology, University of Graz, AF 18010 Graz, Austria*
[d] *Centre for Global Metallogeny, Department of Geology and Geophysics, The University of Western Australia, 35 Stirling Highway, Crawley, W.A. 6009, Australia*
[e] *Department of Geology, University of Assiut, Egypt*

Received 10 January 2001; received in revised form 24 October 2001; accepted 25 November 2001

Abstract

Regional cooling in the course of Neoproterozoic core complex exhumation in the Central Eastern Desert of Egypt is constraint by $^{40}Ar/^{39}Ar$ ages of hornblende and muscovite from Meatiq, Sibai and Hafafit domes. The data reveal highly diachronous cooling with hornblende ages clustering around 580 Ma in the Meatiq and the Hafafit, and 623 and 606 Ma in the Sibai. These $^{40}Ar/^{39}Ar$ ages are interpreted together with previously published structural and petrological data, radiometric ages obtained from Neoproterozoic plutons, and data on sediment dynamics from the intramontane Kareim molasse basin. Early-stage low velocity exhumation was triggered by magmatism initiated at ~650 Ma in the Sibai and caused early deposition of molasses sediments within rim synforms. Rapid late stage exhumation was released by combined effect of strike-slip and normal faulting, exhumed Meatiq and Hafafit domes and continued until ~580 Ma. We propose a new model that adopts core complex exhumation in oblique island arc collision-zones and includes transpression combined with lateral extrusion dynamics. In this model, continuous magma generation weakened the crust leading to facilitation of lateral extrusion tectonics. Since horizontal shortening is balanced by extension, no major crustal thickening and no increase of potential energy (gravitational collapse) is necessarily involved in the process of core complex formation. Core complexes were continuously but slowly exhumed without creating a significant mountain topography.

Keywords: Neoproterozoic; Exhumation; Extension; $^{40}Ar/^{39}Ar$ geochronology; Egypt

1. Introduction

Late orogenic histories are usually associated with extension, exhumation of deeply buried rocks and deposition of sediments adjacent to denudation zones. The lower crust and mantle lithosphere in these orogenic belts may have still being under compression while upper crust had experienced extension. Syn-convergent extension in continental collision zones may by driven by gravitational instabilities (body forces) induced by increase of potential energy known as "gravitational collapse" (e.g., Dewey, 1988; Lister and Davis, 1989; England and Houseman, 1989) or by far-field stresses induced by block motions associated with lateral extrusion (Tapponier and Molnar, 1976; Neubauer et al., 1999). During these processes that are initiated by mechanical instabilities, the velocity of tectonic activity (deformation) is approximately an order of magnitude higher than time required for heat conduction and re-equilibration of the thermally disturbed lithosphere. Consequently short term tectonic processes, rapid exhumation of rocks and clockwise pressure temperature (P–T) metamorphic loops have been predicted and reported from these tectonic settings (England and Thompson, 1984). Granitoids evolve during late stages of extension when removal of a thickened root of cold

* Corresponding author. Tel.: +43-316-380-5579; fax: +43-316-380-9870.
E-mail address: harald.fritz@uni-graz.at (H. Fritz).

0899-5362/02/$ - see front matter
PII: S0899-5362(02)00014-3

lithosphere by convective thinning of the mantle lithosphere or slab-break-off releases both, gravitational instabilities and enhances heat transfer (Houseman et al., 1981; Platt and England, 1994, Davis and Blanckenburg, 1995).

A contrasting evolution characterises oceanic and oceanic/continental convergence zones where large amount of magmas are generated continuously during plate convergence. The amount of vertical material flow is controlled by the horizontal component of the plate velocity perpendicular to the plate boundary (released by far-field stresses), possible lateral extrusion parallel to the plate boundary, and the degree of strike-slip partitioning (Oldow et al., 1990; Teyssier et al., 1995; Tikoff and Teyssier, 1994). During oblique convergence, lithospheric thickening can easily be compensated by orogen-parallel extension and results in an orogen that is not accompanied by significant crustal thickening or topography. In such scenario, body forces do not play a major role during rock exhumation. As documented from ancient as well as from modern island arc settings (e.g. Saint Blanquat et al., 1998), orogenesis is accompanied by continuous magmatism that results in weakening of the lithospheric shear strength, hence facilitating lateral motion. Since gravitational collapse plays only a minor role in this type of tectonic setting magmatism itself can be assumed to be the major driving force for mountain destruction and rocks exhumation. Advectice mass transport that is imposed by emplacement of plutons is balanced by downward movement of cold and dense material resulting in relative vertical mass movement without creating significant topography (England and Molnar, 1990, Warren and Ellis, 1996; Stuewe and Barr, 1998). Since the thermal structure of the lithosphere that was modified by continuous magmatism controls extensional tectonics rather than far-field stresses or body forces, a continuous and slow exhumation process has to be assumed. The corresponding *P–T* metamorphic paths, although highly variable within those orogens (Warren and Ellis, 1996), are defined by a classical anti-clockwise path (Sandiford and Powell, 1990, Sandiford et al., 1991).

In order to identify stress induced from magmatically controlled extension, we focus on the interrelation between extension tectonics, magmatism and depositional dynamics of sedimentary basin during the evolution of Neoproterozoic mountain building in the Central Eastern Desert of Egypt. *P–T* metamorphic paths, kinematic, structural data and sedimentary data relevant to understand the exhumation of core complexes and associated sedimentary basins are reviewed. Time relationships as well as velocities of tectonic and magmatic processes are constrained using published geochronological data and complemented new $^{40}Ar/^{39}Ar$ cooling ages of hornblende and muscovite. We hope to contribute to the understanding of geodynamic processes that drove Neoproterozoic extension in NE Africa by presenting a general model to explain rock exhumation in oblique island arc settings.

2. Geological framework

Many authors have interpreted the Neoproterozoic evolution of the Nubian Shield in NE Africa as a result of accretion of intra-oceanic island arcs, continental micro-plates and oceanic plateaus in the course of consolidation of Gondwana (Gass, 1982; Stern, 1994; Kröner et al., 1994; Abdelsalam and Stern, 1996). Increasing attention has been paid to features associated with extension (Stern et al., 1984; Burke and Sengör, 1986; Wallbrecher et al., 1993; Greiling et al., 1994). A number of core complexes that developed within an extensional regime have been recognised (Sturchio et al., 1983; Fritz et al., 1996; Blasband et al., 2000; Fowler and Osman, 2001). Core complex formation within the Central Eastern Desert of Egypt is closely linked with one of the most spectacular feature within this orogen; the NW-trending Najd Fault System (Stern, 1985). This dominantly sinistral strike-slip system strikes approximately parallel to the orogen over a distance of several hundreds of km. It is exposed, due to disruption by the young Red Sea Rift (Garfunkel, 1988; Omar et al., 1989), in Egypt as well as in Saudi Arabia. Within the Central Eastern Desert of Egypt, core complexes (gneissic domes) namely the Meatiq-, Sibai- and Hafafit dome occur along strike of the Najd Fault System (Fig. 1). They are entirely bound by sinistral strike-slip faults and releasing north- and south-dipping NE-trending normal faults that accommodated exhumation of these core complexes. Those gneissic domes were referred to as "infrastructure" El Gaby et al. (1990). They constitute orthogneisses, psammitic schists and rare amphibolites that suffered amphibolite grade, polyphase metamorphic conditions (Neumayr et al., 1996, Neumayr et al., 1998). Structural cover grouped here as Pan-African Nappes, was referred to as "suprastructure" by El Gaby et al. (1990). These include ophiolites, melange sediments of accretionary wedge-type and calc-alkaline volcanics similar to modern arc magmatism. Metamorphism is of greenschist facies metamorphic grade (Neumayr et al., 1998, Puhl, 1997). Based on the tectonic juxtaposition of low-grade metamorphosed structural cover units against high-grade metamorphosed basement, the gneissic domes have been described as metamorphic core complexes (Sturchio et al., 1983). Neoproterozoic molasse-type basins developed during late orogenic history (Grothaus et al., 1979; Rice et al., 1993; Messner et al., 1996; Fritz and Messner, 1999). These sediments are either incorporated into the Pan-African nappe assembly (Type Hammamat Basin) or were accumulated in intramontane troughs along the

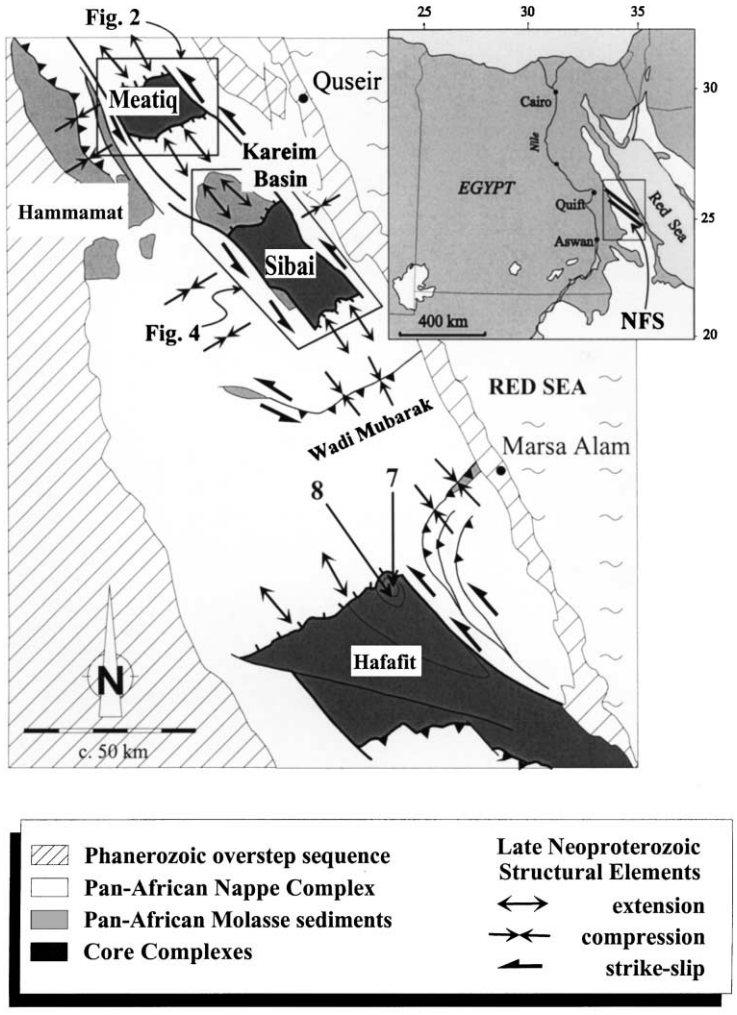

Fig. 1. Metamorphic Core Complexes and molasses-type basins in the Central Eastern Desert of Egypt aligned along the Najd Fault System. Numbers (7, 8) denote sample locations for $^{40}Ar/^{39}Ar$ dating in the Hafafit. In insert map NFS = Najd Fault System.

Najd Fault System (Type Kareim Basin; Fig. 1). Finally extensive granitoid magmatism persisted throughout the Neoproterozoic era of the Nubian Shield in the Eastern Desert of Egypt.

The structural assembly in the Central Eastern Desert has been interpreted as a result of oblique convergence that partitioned into an internal wrench corridor represented by the Najd Fault System and a western fold and thrust belt (Fritz et al., 1996; Fritz and Messner, 1999). While thrusts propagated westward to incorporate the Hammamat molasse sediments into the nappe edifice (Fig. 1), extension occurred simultaneously within the Najd Fault System. Exhumation of internal core complexes accompanied NW–SE sinistral strike-slip faulting that resulted in NW–SE directed extension which provided depocentres for the accumulation of intramontane molasse basins of the Kareim Basin Type (Fig. 1) (Fritz and Messner, 1999) as well as weak zones for the intrusion of granitoid rocks. Approximately 30% of surface outcrops within the Meatiq core complex and 90% of the Sibai core complex constitute granitoid rocks.

The Neoproterozoic evolution of the Arabian Nubian Shield includes: (1) ophiolites interpreted as oceanic crust which formed by rifting of Rodinia (Abdelsalam and Stern, 1996). The ages of the ophiolites range between 900–740 Ma (Ries et al., 1983; Kröner, 1985; Kröner et al., 1992, 1994; Loizenbauer et al., 2001); (2) Development of sutures associated with arc accretion that occurred between ~750–650 Ma (Abdelsalam and Stern, 1996; Blasband et al., 2000); and (3) Late orogenic extension and exhumation of core complexes constrained by radiometric ages on core complex exhumation (Fritz et al., 1996), estimates on molasse basin formation (Grothaus et al., 1979; Rice et al., 1993, Willis et al., 1988) and ages of late to post-tectonic magmatic activity (Sturchio et al., 1993; Stern and Hedge, 1985; Hassan and Hashad, 1990). The data suggest close association between tectonic and magmatic activity at 620–580 Ma as will be discussed below.

3. Extension in the Central Eastern Desert

NW–SE directed extension in the Central Eastern Desert exhumed a number of basement complexes, namely the Meatiq-, Sibai-, and Hafafit dome and resulted in the formation of the Kareim intramontane molasse basin (Fig. 1) between the Meatiq and the Sibai. Extensional structures are very similar throughout the belt including sinistral strike-slip shear zones and NW- and SE-dipping normal faults (Figs. 1, 2 and 4). However, exhumed rock types and the interplay between magmatic and tectonic activities is very different. In the Meatiq dome and Hafafit dome gneisses dominate and only a limited amount of late- to post-extensional granitoids are exposed (El Gaby et al., 1990; Rashwan, 1991; Greiling et al., 1994; Neumayr et al., 1995; Neumayr et al., 1996; Neumayr et al., 1998). On the other hand the Sibai dome is made up almost entirely of late Pan-African plutons (Kamal El Din, 1993; Khudeir et al., 1995; Greiling et al., 1994, Bregar, 1996).

3.1. The Meatiq core complex

A discussion on the complex metamorphic and magmatic history of the Meatiq dome is beyond the scope of this study. The focus is on the late Neoproterozoic evolution dominated by of extensional tectonics. Along the southern margin of the Meatiq core complex the sheet-like calc-alkaline Abu Ziran granitic body intruded between the Meatiq structural basement and the detached structural cover rocks of the Pan-African Nappe Complex (Fig. 2). This syn-extensional emplacement has been documented by studying the relationship between magmatism and solid state flow (Fritz et al., 1996; Fritz and Puhl, 1996). It has been shown that the regional NW–SE directed extension opened space that was progressively sealed with different magmatic phases ranging from mafic precursor rocks to tonalites and granodiorites (Fritz and Puhl, 1996). Thermal metamorphic aureoles had been identified especially within the southern adjacent Pan-African Nappes. The contact aureole itself was disturbed by NW–SE directed extension. To the north of the Abu Ziran granitoid, exhumed ''hot'' rocks of the Meatiq core complex have bee juxtaposed against the pluton and only a narrow aureole was developed. Barometric data from mafic enclaves, based on Altot content of hornblende (Schmidt, 1992), suggest early magma crystallisation at ~14 km depth (~5 kbar, Fritz and Puhl, 1996). The 614 ± 8 Ma U/Pb zircon crystallisation age (Stern and Hedge, 1985) is thus interpreted to date mid-crustal extension in the Meatiq. Sinistral strike-slip movement along shear zones that produced extension has been dated by newly grown, syn-tectonic white mica that gave $^{40}Ar/^{39}Ar$ ages of 588 Ma and 595 Ma (Fritz et al., 1996). The upper limit of the Neoproterozoic tectonic activity in the Meatiq is given by circular shaped, post-tectonic Arieki granitoid that gave an whole rock Rb/Sr age of 579 ± 6 Ma (Hassan and Hashad, 1990).

P–T evolutionary paths using conventional cation exchange thermobarometer combined with fluid inclusion studies have been established for the Meatiq structural basement (core complex) as well as for Pan-African nappes next to the Abu Ziran granitoid (Puhl, 1997; Neumayr et al., 1995, 1998; Loizenbauer, 1998; Loizenbauer et al., 2001). Entrapment of individual fluid generations had been carefully correlated with tectonic events. These studies indicate that the internal portions of the Meatiq core complex (Fig. 3, path 1) exhibit peak metamorphic conditions of ~750 °C and ~8 kbar fol-

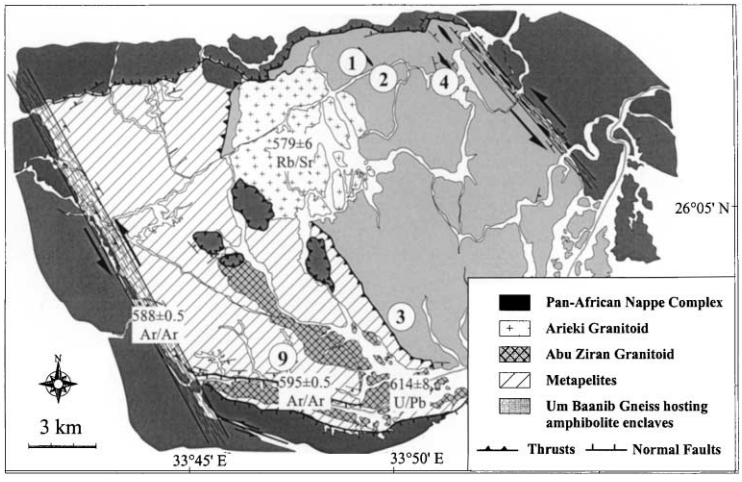

Fig. 2. Simplified map of the Meatiq Core Complex. Locations sampled for $^{40}Ar/^{39}Ar$ age determination are indicated by the numbers 1, 2, 3, 4, 9. $^{40}Ar/^{39}Ar$ ages of 588 and 595 Ma interpreted to date exhumation related to strike-slip and normal faults are from Fritz et al. (1996). Crystallisation ages of 614 Ma from the syn-extensional Abu Ziran Pluton is from Stern and Hedge (1985) and the age of 579 Ma from the post-tectonic Arieki pluton is from Hassan and Hashad (1990).

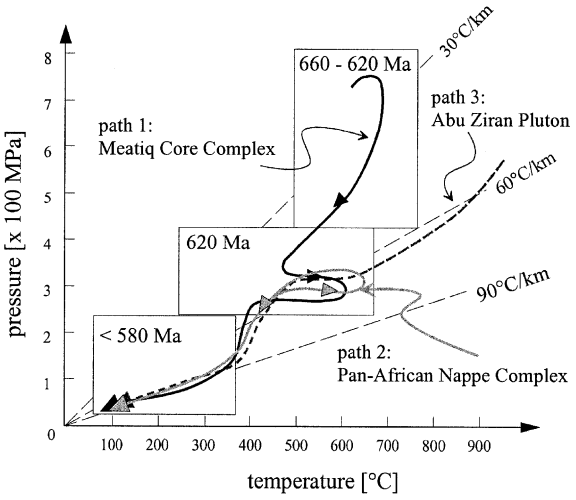

Fig. 3. Pressure–temperature–time paths of the Meatiq Core Complex (path 1), the Pan-African Nappe Complex next to the Abu Ziran pluton (path 2), and the Abu Ziran pluton (path 3). Data are compiled from Fritz and Puhl (1996), Puhl (1997), Neumayr et al. (1998), Loizenbauer (1998) and Loizenbauer et al. (2001).

lowed by a moderate decrease of pressures and temperatures down to 4–5 kbar and 450 °C. Next to the Abu Ziran pluton, rocks were advectively heated and subsequently experienced isobaric cooling at ~4 kbar. Late stages of exhumation are characterised by a steep pressure gradient as shown by decrepitation features of late aqueous fluid inclusions. Structural cover units represented by the Pan-African Nappe Complex were affected by greenschist metamorphic conditions at ~450 °C and 4 kbar although temperature peak of 640 °C had been reached along the pluton/host-rocks interface. Subsequent to advective heating, both pluton and host rocks once more suffered isobaric cooling followed by moderate decompression during final exhumation (Fig. 3, Path 2).

Extensional events in the Meatiq area can be summarised as follow: (1) moderate extension started in mid-crustal level before 614 Ma resulting in exhumation of rocks of the Meatiq core complex from ~20 km depth to ~14 km depth; (2) isobaric cooling at down to ~400 °C around 614 Ma; and (3) final exhumation rapidly exposed rocks from ~10 km close to surface levels around 590 Ma.

3.2. The Sibai core complex and Kareim Sedimentary Basin

Approximately 90% of the Sibai core complex (Fig. 4) is made-up of Neoproterozoic granitoid rocks of calc-alkaline to alkaline chemical affinity (Kamal El Din, 1993; Khudeir et al., 1995; Bregar, 1996). Pre-granitic host rocks are limited to rare lenses of amphibolites. The Pan-African Nappes Complex includes serpentinites and melange-type sediments that are tectonically imbricated together with deformed granitoids such as El Shush Gneiss of modern arcs chemical affinity. Single zircon

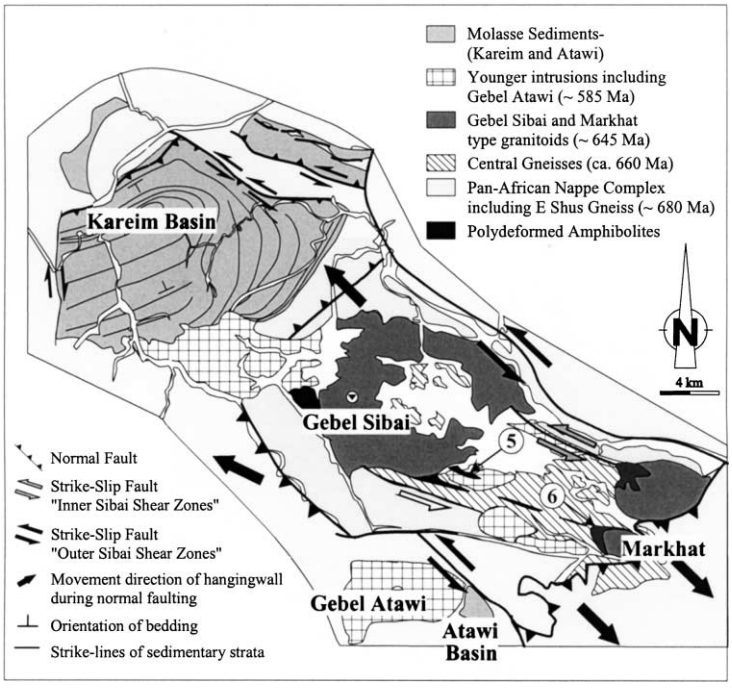

Fig. 4. Simplified map of the Sibai Core Complex and the Kareim sedimentary basin including sample locations for $^{40}Ar/^{39}Ar$ data (5, 6) (modified after Fritz and Messner, 1999). Basin subsidence within the Kareim sedimentary basin (strike-line contours are inserted) to the north of the Sibai dome was accomplished by NE–SW trending normal faults and was coeval with final exhumtion of the Sibai core complex (for details see text).

evaporation ages from the El Shush Gneiss, interpreted as magmatic ages (Bregar, 1996) indicate that the accretionary stage of Pan-African orogenesis in the Sibai occurred at ~680 Ma.

Succession and relative timing of deformational phases during extension and exhumation of the Sibai rocks is constraint by interrelations between magmatic and tectonic events (all geochronological ages in this section were obtained from $^{207}Pb/^{206}Pb$ single zircon evaporation techniques and are average values of data from 4–6 individual zircons). During the first stage of the NW–SE directed extension vertically foliated diorites with magmatic ages of ~660 Ma intruded the central parts of the Sibai (Bregar, 1996). These "Central Gneisses" (Fig. 4) are elongated in a NW–SE direction and are bounded by the sinistral "Inner Sibai Shear Zones" along their southwestern and northeastern margins. To the southeast and northwest of the Sibai, the Central Gneisses and shear zones are discordantly cut by younger granitoids of within-plate chemical affinity and extensional shear zones defining a second stage of extensional tectonics. These granitoids are represented by the Abu Markhat and Abu Sibai intrusions which gave crystallisation ages ranging between 650 and 640 Ma. The extensional shear zones are associated with a younger phase of sinistral strike-slip faulting referred to as "Outer Sibai Shear Zones" that post-dates pluton emplacement. A younger suite of highly differentiated late- to post-tectonic granitoids occurs as isolated bodies within the Sibai as well as along its margins. Along the southwestern Sibai margin the ~580 Ma (Rb/Sr) Atawi granitoid (Fig. 4; Hassan and Hashad, 1990) was deformed by post-emplacement sinistral strike-slip shearing. The emplacement of this pluton was synchronous with deposition of a small pull-apart molasse basin (Pelz, 1996).

Exhumation of the Sibai has its manifestation on the sedimentary record within the northerly adjacent Kareim Molasse Basin (Fig. 4). Basin subsidence and sedimentary delivery rates in the basin point to several denudation stages of the to the Sibai dome. Approximately 7000 m of siliciclastic sediments, dominantly transported from the Sibai swell in the south have been deposited in prevalent lacustrine and braided stream environments to the north (Fritz and Messner, 1999). The synform geometry of the basins is displayed by S-dipping strata in the north, steeply N-dipping strata in the south, and a generally W–E trending basin axes. Sinistral strike-slip faults of the outer set of shear zones in the Sibai transsect the basin along its northeastern margin (Fig. 4). Sedimentary facies and component analyses have been used to constrain subsidence history of the basin. The subsidence history of the basin in turn has been correlated with the exhumation history of the Sibai Core Complex (Fritz and Messner, 1999). It is concluded that transport energy of sediments was provided by the average height of relief between the depocenter (synform trough) and the source area of the clastic sediments (Sibai exhumation).

Three major sedimentary events (megacycles) have been distinguished in the Kareim Basin (Fig. 5): (1) basin formation started with constant shallow water lacustrine facies that was characterised by low sedimentation rates. Subsequent increase in relief energy resulted in deposition of coarse grained fluviatile sediments on top of the sequence, hence an upwards coarsening megacycle; (2) sediment delivery and relative denudation of hinterland decreased progressively resulting in deposition of lacustrine sediments, an upwards fining megacycle; (3) sudden change in depositional environment is indicated by accumulation of very coarse alluvial fanglomerates signalising a phase of rapid subsidence and high sediment delivery rates during late-stage sedimentary evolution.

The sedimentary facies and subsidence history of the Kareim Basin suggest minor vertical uplift of the hinterland during early stages of basin formation. This was followed by gradual increase in relief energy as indicated by the upward coarsening megacycle. Subsequently, exhumation process within the hinterland decreased and progressively fine-grained sediments were delivered. It is suggested that magmatically-driven subsidence during the early stage of basin formation (Fig. 5) was induced by extraction and uprise of northern Sibai granitoids. This was balanced by downward movement of cold and dense material and formed a rim syncline, similar to what has been suggested by Weinberg and Podladchikov (1995), Warren and Ellis (1996) and Fritz and Messner (1999). This scenario is supported by illite crystallinity data from the Kareim basin that cluster around 0.24 (full-width at half-height at 10 Å: Fritz and Messner, 1999) which suggest high thermal gradient and/or contribution of heat by magma advection. Late stage subsidence and basin modification was tectonically driven (Fig. 5) and was triggered by a combination of strike-slip and normal faulting (Fritz and Messner, 1999; Kamal El Din, 2000). Very high subsidence rates and extensive erosion of a granitic source characterise this stage.

There are no age constraints for the Kareim Basin. Willis et al. (1988) used a whole rock Rb/Sr age of 585 ± 15 Ma from Hammamat sediments north to the study area to infer the age of deposition. An age of ~585 Ma is suggested for the late stage sedimentary evolution. The ~585 Ma Gebel Atawi granitoid which was emplaced along the Outer Sibai Shear zone is approximately coeval with the formation of a small pull-apart basin (Pelz, 1996). The southern margin of the Kareim basin is intruded by a late magmatic body of a presumable late Neoproterozoic age. Nevertheless, we emphasise that timing of events of molasses-type sedimentation may differ significantly in the Eastern Desert from one basin to another (Messner et al., 1996).

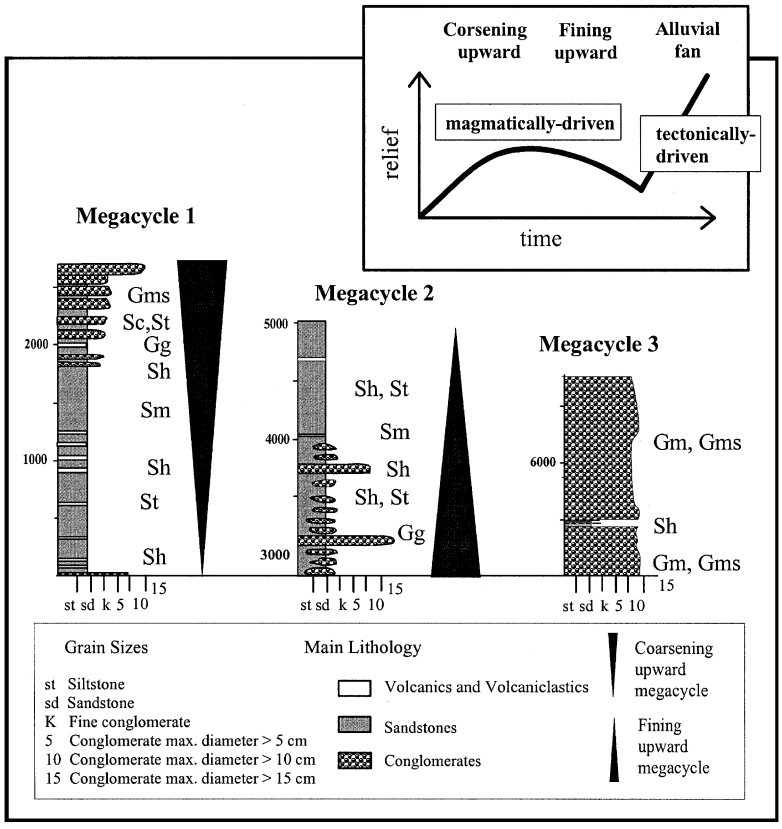

Fig. 5. Stratigraphic columns of the Kareim basin (modified after Fritz and Messner, 1999) including grain size distribution, main lithological units, sedimentary facies and depositional environment (classification after Postma (1990)). Gm: high density mass flows; Gms: sheet flow, stream flow; Gg: channel flow; Sm: rapid suspension fallout; Sh: planar bed flows; St: dunes, lower flow regime, Sc: scour fills.

Data from the Sibai dome and the Kareim basin suggests that: (1) The Neoproterozoic accretionary phase in the Sibai continued until 680 Ma. (2) NW–SE directed extension initiated at ~660 Ma together with emplacement of Central Gneisses in mid crustal levels. Major vertical rock flow might have not accompanied this phase. (3) Moderate exhumation of the Sibai and delivery of sediments to the Kareim basin initiated at ~645 Ma and was accompanied by extensive magmatic activity such as intrusion of the Gebel Sibai and Gebel Markhat granitoids suggesting magmatically-induced exhumation. (4) The major rapid exhumation phase and extension within a dominant strike-slip setting suggests a tectonically induced exhumation that occurred after 645 Ma and continued until 580 Ma.

4. The cooling history

Exhumation was highly diachronous in the Central Eastern Desert reflecting a long term tectonic process that was closely related to intensive magmatic activity. In the Meatiq core complex, tectonic and magmatic history related to exhumation processes between ~614 Ma and 580 Ma contrast that of the Sibai area. In Sibai extension started with emplacement of within-plate granitoids at ~660 Ma followed by exhumation at ~645 Ma. In order to obtain age data on the late-stage cooling histories, $^{40}Ar/^{39}Ar$ age determinations on hornblende and white mica from Meatiq-, Sibai- and Hafafit domes were performed. Sample locations are shown in Figs. 1, 2, 4, and 8.

4.1. Analytical procedure

Hornblende and white mica concentrates were wrapped in aluminium-foil packets, encapsulated in sealed quartz vials, and irradiated for 40 h in the central thimble position of the TRIGA Reactor in the US Geological Survey, Denver. Variation in the flux of neutrons along the length of the irradiation assembly was monitored with several mineral standards, including MMhb-1 (Samson and Alexander, 1987). The samples were incrementally heated until fusion in a double-vacuum, resistance heat furnace. Temperatures were monitored with a direct-contact thermocouple and are controlled to ±1 °C between increments and are accurate to ±5 °C. Measured isotopic ratios were corrected for total blanks and the effects of mass discrimination. Interfering isotopes produced during irradiation were

corrected using factors reported by Dalrymple et al. (1981) for the TRIGA Reactor. Apparent $^{40}Ar/^{39}Ar$ ages were calculated from corrected isotopic ratios using the decay constants and isotopic ratios listed by Steiger and Jäger (1977) following the methods described in Dallmeyer and Takasu (1992). The intralaboratory uncertainties (1σ) reported here have been calculated by statistical propagation of uncertainties associated with measurement of each isotopic ratio through the age equation. The interlaboratory uncertainties are $\sim\pm1.25$–1.5% of the quoted age. Total-gas ages have been computed for each sample by appropriate weighting of the age and percent ^{39}Ar released within each temperature increment. A ''plateau'' is considered to be defined if the ages recorded by two or more continuous gas fractions each representing $>4\%$ of the total ^{39}Ar evolved are mutually similar within a $\pm1\%$ interlaboratory uncertainty. A detailed description of the procedure is given in Dallmeyer et al. (1992).

4.2. The geochronological data

Hornblende concentrates were prepared from amphibolites collected from the Meatiq core complex (samples 1–4), from the Sibai (samples 5 and 6), and from the Hafafit (samples 7 and 8). One muscovite concentrate has been obtained from the Meatiq core complex (sample 9). Age spectra are shown in Fig. 6. Analytical data are provided in Table 1 (samples 1 and 2). The hornblende concentrates display variably discordant $^{40}Ar/^{39}Ar$ age spectra (Fig. 6). The relatively small volume low-temperature gas fractions indicate considerable variation in apparent ages. These are matched by fluctuations in apparent K/Ca ratios which suggest that experimental evolution of argon occurred from compositionally distinct, relatively non-retentive phases. These could be represented by: (1) very minor optically undetectable mineral contaminants in the hornblende concentrates; (2) petrographically unresolved exsolution or compositional zonation within constituent hornblende grains; and/or (3) intracrystalline inclusions. Most intermediate- and high-temperature gas fractions display little intra-sample variation in apparent K/Ca ratios, suggesting experimental evolution of gas occurred from compositionally uniform sites.

4.3. Horblende and white mica from the Meatiq dome

The optically unzoned hornblende crystals in the concentrates from samples 1–4 have been derived from migmatitic amphibolites that occur in schollen within the Um Baanib gneiss (Fig. 2). These rocks suffered a polyphase metamorphic history (Neumayr et al., 1995, 1999). They have been deformed and migmatised prior to 780 Ma, intruded by the Um Baanib gneiss at $\sim$ 780 Ma and incorporated into the Pan-African Nappe Complex around 660 Ma (Loizenbauer et al., 2001).

The intermediate- and high-temperature increments (820 °C-fusion) evolved from samples 1, 3, 4 do not rigorously define a plateau. However, the apparent ages display relatively little variation within the sample, and a $^{36}Ar/^{40}Ar$ vs. $^{39}Ar/^{40}Ar$ isotope correlation of these data are well defined. The inverse ordinate intercept ($^{40}Ar/^{36}Ar$ ratio) is only slightly larger than the $^{40}Ar/^{36}Ar$ ratio in the present-day atmosphere and suggests therefore only minor intracrystalline contamination with extraneous argon components. The plateau ages of all hornblende concentrates are very similar (579–587 Ma) and close to the 588–595 Ma $^{40}Ar/^{39}Ar$ white mica ages obtained from shear zones that accommodated exhumation of the Meatiq core complex (Fritz et al., 1996). Thus the obtained data are considered geologically significant and interpreted to date post-metamorphic cooling through temperatures required for intracrystalline retention of radiogenic argon in constituent hornblende grains. Harrison (1981) suggested that temperatures of $\sim 500 \pm 25$ °C are appropriate for argon retention within most magmatic hornblende compositions in the range of cooling rates likely to characterise most geologic settings. However, closure temperatures for metamorphic hornblende might be slightly lower because of their more complicated mineralogy compared to magmatic ones (Onstott and Peacock, 1987; Baldwin et al., 1990).

Muscovites derived from sample 9 (Fig. 6) is part of the high temperature mineral assembly of garnet-kyanite bearing metapelites 4 km north of the southern margin of the Meatiq dome (Fig. 2). Peak metamorphic conditions of $\sim$750 °C and 8 kbar subsequently followed by decompression down to 4–5 kbar (Neumayr et al., 1998) was associated with localised extensional shear zones along the southern margin of the Meatiq dome. All gas fractions evolved from the muscovite concentrates were characterised by very large apparent K/Ca ratios. These display no significant or systematic intra-sample variations. Therefore, apparent K/Ca spectra are not presented with the apparent age spectra in Fig. 6. The muscovite concentrate is characterised by internally concordant $^{40}Ar/^{39}Ar$ age spectra which define a plateau age of 582 Ma. The $^{40}Ar/^{39}Ar$ plateau age is interpreted to date cooling through temperatures required for argon retention in the course of Meatiq core complex exhumation. Although not rigorously calibrated experimentally, using the experimental data of Robbins (1972) in the diffusion equations of Dodson (1973) suggests that temperatures of $\sim$375–400 °C may be appropriate for argon retention in muscovites of normal composition. These calculations depend highly on the diffusion geometry within mica and may be overestimated. Recently Hames and Bowring (1994) proposed a cylindrical diffusion geometry with an effective diffusion dimension

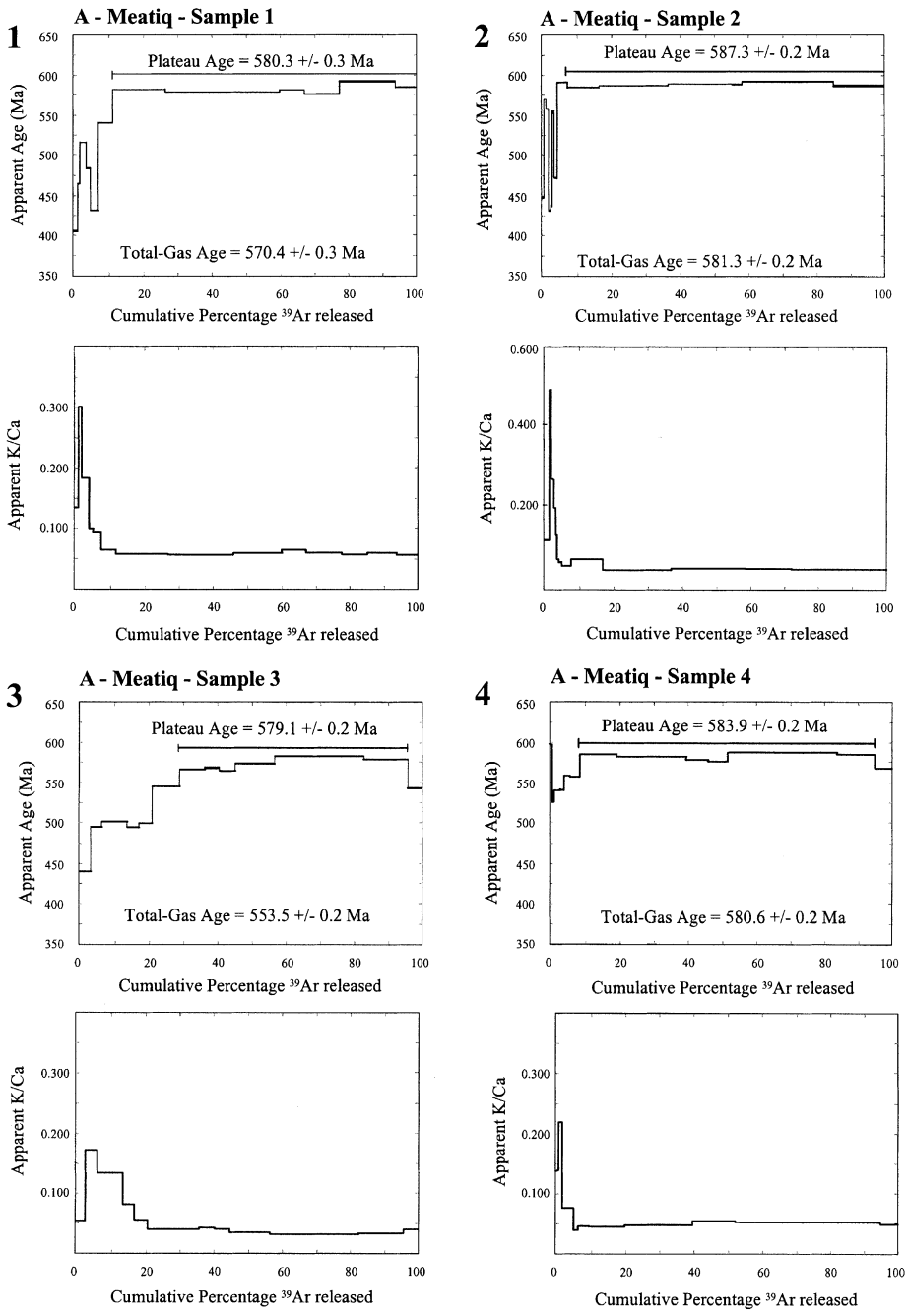

Fig. 6. The $^{40}Ar/^{39}Ar$ incremental-release age and apparent K/Ca spectra for hornblende concentrates from (A) the Meatiq Core Complex (samples 1, 2, 3, 4, and 9); (B) the Sibai Core Complexes (samples 5 and 6); and (C) the Hafafit Core Complex (samples 7 and 8). For sample locations see Figs. 1, 2 and 4. Analytical uncertainties (intra-laboratory) shown by the vertical width of bars. The inter-laboratory uncertainties are ca. ±1.25–1.5% of the quoted age.

equal to the crystal diameter. Cliff (1985) and Blanckenburg et al. (1989) and McDougall and Harrison (1999) estimated closure temperatures of ~350–410 °C as appropriate temperatures for argon retention within white mica based on field studies.

Hornblende (579–587 Ma) and muscovite cooling ages (582 Ma) are very similar and may reflect rapid cooling form temperatures exceeding 500 °C down to 350 °C.

4.4. Hornblende from the Hafafit dome

Two hornblende concentrates have been separated from ortho-gneisses exposed in the central portions of the Hafafit gneiss culmination that host diorite and tonalite schollen (Greiling et al., 1994; Kröner et al., 1994). Previous geochronological data from Hafafit suggest emplacement of trondhjemites which are part of an I-type calc-alkaline assembly at ~700 Ma

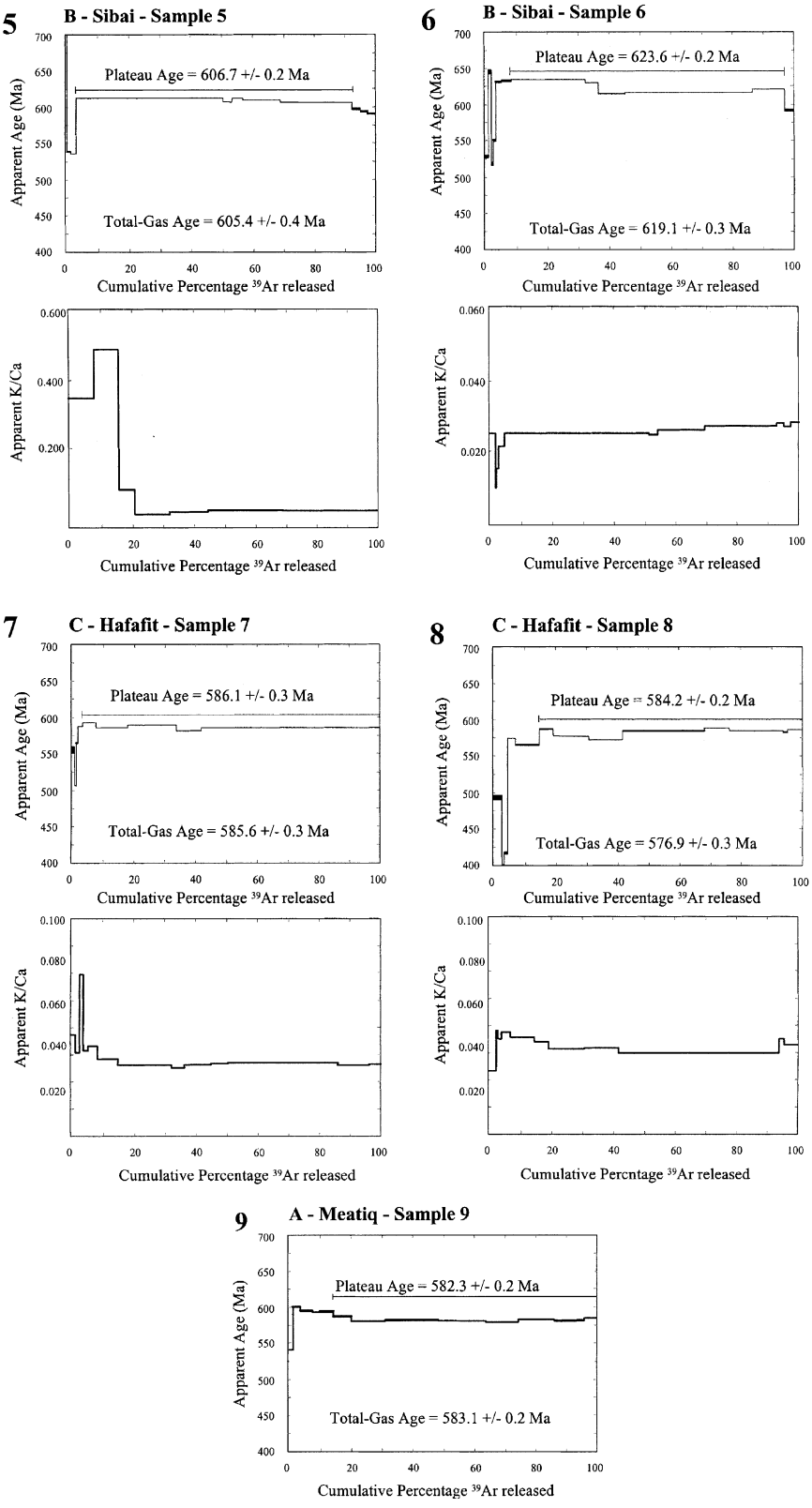

Fig. 6 (*continued*)

($^{207}Pb/^{206}Pb$ single zircon evaporation ages: Kröner et al., 1994). Crystallisation ages from the granitoid gneisses are 682 Ma (Stern and Hedge, 1985), 698 Ma and 700 Ma (Kröner et al., 1994). These ages are close to the

Table 1
$^{40}Ar/^{39}Ar$ analytical data for incremental heating experiments on hornblende and muscovite concentrates from the Eastern Desert of Egypt

Release temperature (°C)	($^{40}Ar/^{39}Ar$)[a]	($^{36}Ar/^{39}Ar$)[a]	($^{37}Ar/^{39}Ar$)[c]	^{39}Ar % of total	% ^{40}Ar non-atmos.+	$^{36}Ar_{Ca}$ (%)	Apparent Age (Ma)[b]
Sample 1: Hornblende from amphibolite schollen within the Um Baanib gneiss (Meatiq) J = 0.009015							
600	102.71	0.25426	3.672	0.85	27.13	0.39	405.1 ± 0.9
700	46.14	0.04623	1.620	0.79	70.66	0.95	465.2 ± 0.3
800	43.71	0.02439	2.659	1.80	83.99	2.96	516.5 ± 0.3
850	41.00	0.02493	4.815	1.36	82.96	5.25	483.8 ± 0.6
875	38.17	0.02943	5.160	2.20	78.29	4.77	431.5 ± 0.5
900	41.65	0.01243	7.396	4.48	92.59	16.18	540.4 ± 0.2
925	43.13	0.00623	8.645	15.22	97.33	37.76	581.7 ± 0.4
950	42.50	0.00540	8.755	19.29	97.88	44.06	577.2 ± 0.3
975	42.55	0.00559	8.497	14.10	97.71	41.35	576.9 ± 0.3
1000	42.03	0.00277	7.835	7.20	99.53	76.82	579.7 ± 0.1
1025	42.48	0.00603	8.459	10.36	97.39	38.16	574.4 ± 0.2
1050	43.24	0.00473	8.866	7.65	98.40	50.96	588.5 ± 0.3
1100	42.94	0.00339	8.591	8.91	99.26	68.93	589.3 ± 0.2
Fusion	42.94	0.00433	9.230	5.78	98.72	57.95	582.0 ± 0.3
Total	43.07	0.00903	8.223	100.00	96.11	43.92	570.4 ± 0.3
Total without 600–900 °C				88.51			580.3 ± 0.3
Sample 2: Hornblende from amphibolite schollen within the Um Baanib gneiss (Meatiq) J = 0.009791							
600	99.01	0.23918	3.987	1.02	28.94	0.49	447.0 ± 0.8
700	41.91	0.01423	1.003	0.80	90.07	1.90	567.6 ± 0.3
750	39.66	0.01011	1.817	0.69	92.82	4.89	555.8 ± 0.2
800	39.24	0.04032	2.431	0.58	70.13	1.64	413.0 ± 1.0
825	31.62	0.01338	3.598	0.52	88.39	7.31	437.1 ± 1.0
850	38.66	0.00915	6.227	0.50	94.29	18.51	552.3 ± 1.3
875	37.23	0.02515	6.931	0.96	81.52	7.50	471.2 ± 1.1
900	39.58	0.00344	8.102	2.72	99.06	64.01	588.6 ± 0.2
925	40.29	0.00908	6.313	9.35	94.58	18.90	573.9 ± 0.1
950	39.64	0.00514	9.225	19.86	98.03	48.85	584.5 ± 0.2
975c	39.55	0.00385	8.664	18.42	98.87	61.23	587.5 ± 0.2
1000	39.44	0.00357	8.351	2.82	99.02	63.70	586.7 ± 0.4
1050	39.71	0.00374	9.041	26.47	99.03	65.76	590.5 ± 0.2
Fusion	39.77	0.0508	8.664	15.30	97.96	46.42	585.6 ± 0.2
Total	40.26	0.00774	8.348	100.00	96.98	51.05	781.3 ± 0.3
Total without 600–925 °C				82.87			587.3 ± 0.2
Sample 3: Hornblende from amphibolite schollen within the Um Baanib gneiss (Meatiq) J = 0.009235							
600	79.77	0.17168	8.862	3.47	37.29	1.40	440.1 ± 0.5
700	42.61	0.02963	2.826	3.18	79.97	2.59	494.4 ± 0.1
800	38.63	0.01467	3.640	7.33	89.53	6.75	501.6 ± 0.1
850	37.05	0.01189	5.883	3.38	91.78	13.46	494.2 ± 0.2
875	39.50	0.01968	8.552	3.90	86.99	11.78	499.6 ± 0.2
900	41.57	0.01523	11.838	8.14	91.44	21.14	546.3 ± 0.2
925	40.42	0.00558	11.905	7.11	98.28	58.06	567.5 ± 0.2
950	37.90	0.00336	10.912	4.40	99.69	88.23	543.1 ± 0.3
975	39.66	0.00341	11.831	4.54	99.84	94.31	565.8 ± 0.2
1000	40.76	0.00549	13.446	11.37	98.66	66.64	573.9 ± 0.3
1050	41.92	0.00724	14.612	26.05	97.68	54.86	583.2 ± 0.2
1100	42.20	0.00872	13.684	13.06	96.48	42.57	580.2 ± 0.2
Fusion	40.99	0.01393	12.088	4.08	92.32	23.61	544.3 ± 0.3
Total	42.21	0.01530	11.637	100.00	93.27	23.61	553.3 ± 0.2
Total without 600–950 °C and fusion				55.02			579.1 ± 0.2
Sample 4: Hornblende from amphibolite schollen within the Um Baanib gneiss (Meatiq) J = 0.009505							
600	145.62	0.35407	3.427	0.85	28.34	0.26	598.1 ± 1.4
700	62.13	0.08991	2.195	0.73	57.51	0.66	528.1 ± 0.2
800	50.18	0.04736	6.284	1.46	73.11	3.61	541.5 ± 0.3

(*continued on next page*)

Table 1 (*continued*)

Release temperature (°C)	(^{40}Ar/^{39}Ar)[a]	(^{36}Ar/^{39}Ar)[a]	(^{37}Ar/^{39}Ar)[c]	^{39}Ar % of total	% ^{40}Ar non-atmos.+	$^{36}Ar_{Ca}$ (%)	Apparent Age (Ma)[b]
850	49.92	0.04618	6.312	1.46	73.67	3.72	542.7 ± 0.4
875	41.11	0.01380	12.742	1.75	92.56	25.11	560.8 ± 0.4
900	41.48	0.01496	11.105	2.83	91.48	20.19	559.0 ± 0.2
925	41.59	0.00798	11.300	10.78	96.50	38.49	586.5 ± 0.2
950	41.01	0.00679	11.185	20.15	97.29	44.81	583.5 ± 0.2
975	40.45	0.00548	9.696	6.47	97.91	48.14	579.4 ± 0.1
1000	40.70	0.00678	9.457	5.75	96.93	37.94	577.5 ± 0.2
1050	41.02	0.00498	10.137	31.91	98.38	55.32	588.9 ± 0.3
1100	40.95	0.00889	10.194	11.30	95.57	31.18	573.7 ± 0.1
Fusion	41.38	0.01190	11.157	4.56	93.65	25.49	569.2 ± 0.4
Total	42.36	0.01181	10.305	100.00	95.93	41.94	580.6 ± 0.2
Total without 600–900 °C and fusion				86.36			583.9 ± 0.2
Sample 5: Hornblende from amphibolite lenses within the Sibai J = 0.009552							
600	222.47	0.56989	19.264	1.05	25.00	0.92	776.1 ± 9.4
700	83.60	0.11520	47.181	0.17	63.81	11.14	761.4 ± 3.7
800	63.68	0.10305	31.437	0.92	56.14	8.30	539.2 ± 0.8
850	51.36	0.05896	22.523	1.99	69.59	10.39	526.4 ± 0.3
900	43.00	0.00953	19.585	46.67	97.10	55.92	611.9 ± 0.2
925	41.90	0.00728	19.890	2.83	98.67	74.33	606.7 ± 0.2
950	42.29	0.00691	18.960	3.50	98.76	74.64	611.7 ± 0.2
975	42.08	0.00683	18.847	11.85	98.79	75.06	609.3 ± 0.3
1000	41.61	0.00906	18.318	23.68	97.09	55.01	594.5 ± 0.2
1025	40.94	0.01362	17.738	2.35	93.64	35.43	568.3 ± 0.3
1050	42.26	0.00692	18.360	2.02	98.64	72.14	610.5 ± 0.4
Fusion	40.08	0.00494	17.576	2.98	98.86	96.69	589.6 ± 0.9
Total	44.66	0.01674	19.267	100.00	95.70	58.22	605.4 ± 0.4
Total without 600–850 °C and 1025 °C-fusion				88.52			606.7 ± 0.2
Sample 6: Hornblende from the Abu Markhat gneiss (Sibai) J = 0.009782							
600	131.29	0.33013	10.522	1.52	26.34	0.87	528.5 ± 2.2
700	68.28	0.08706	12.851	0.81	63.83	4.01	644.9 ± 2.0
750	51.55	0.06235	8.985	0.37	65.65	3.92	518.3 ± 2.0
800	41.22	0.01828	6.604	1.15	88.17	9.83	550.7 ± 1.4
850	49.30	0.02649	12.630	1.67	86.17	12.97	631.0 ± 1.0
875	43.35	0.01745	11.962	3.11	90.31	18.65	588.6 ± 0.4
900	44.92	0.01108	13.943	6.60	95.19	34.23	635.0 ± 0.3
925	44.68	0.01081	14.979	17.22	95.53	37.69	634.5 ± 0.2
950	44.06	0.00982	15.662	4.22	96.26	43.40	631.2 ± 0.3
975	42.67	0.00870	14.845	8.27	96.76	46.41	616.8 ± 0.1
1000	42.06	0.00604	14.685	5.63	98.55	66.13	618.8 ± 0.2
1050	42.21	0.00674	14.584	35.60	98.05	58.88	618.0 ± 0.2
1100	43.18	0.00894	14.869	10.39	96.63	45.22	622.3 ± 0.2
Fusion	44.35	0.02053	14.918	3.43	89.00	19.64	593.7 ± 0.8
Total	44.84	0.01526	14.417	100.00	94.77	45.45	619.1 ± 0.3
Total without 600–875 °C and fusion				87.93			623.6 ± 0.2
Sample 7: Hornblende from orthogneisses within the Hafafit J = 0.009784							
600	119.73	0.28135	4.341	0.58	30.85	0.42	557.7 ± 1.2
700	47.92	0.05182	4.205	0.26	68.74	2.21	505.0 ± 0.7
800	50.52	0.04628	6.146	0.81	73.90	3.61	563.4 ± 0.6
850	42.58	0.01371	6.412	1.37	91.68	12.72	585.5 ± 0.1
875	40.59	0.00548	6.007	4.33	97.19	29.83	590.5 ± 0.2
900	39.59	0.00354	5.963	10.48	98.55	45.84	585.0 ± 0.3
925	39.52	0.00225	5.960	15.66	99.51	72.04	589.0 ± 0.4
950	38.85	0.00226	5.703	8.30	99.44	68.61	580.0 ± 0.3

Table 1 (*continued*)

Release temperature (°C)	(^{40}Ar/^{39}Ar)[a]	(^{36}Ar/^{39}Ar)[a]	(^{37}Ar/^{39}Ar)[c]	^{39}Ar % of total	% ^{40}Ar non-atmos.+	$^{36}Ar_{Ca}$ (%)	Apparent Age (Ma)[b]
975	39.57	0.00317	5.918	21.74	98.82	50.83	586.1 ± 0.2
1000	39.51	0.00290	5.795	17.16	98.99	54.30	586.2 ± 0.2
1050	39.47	0.00285	5.860	13.12	99.05	55.98	585.9 ± 0.3
Fusion	39.84	0.00398	5.962	6.18	98.23	40.72	586.5 ± 0.2
Total	40.16	0.00529	5.884	100.00	98.13	53.52	585.5 ± 0.2
Total without 600–850 °C				96.98			586.1 ± 0.3
Sample 8: Hornblende from orthogneisses within the Hafafit J = 0.009792							
600	238.49	0.70416	16.523	2.53	13.31	0.64	492.6 ± 3.9
700	69.65	0.15977	10.032	0.47	33.37	1.71	372.0 ± 1.5
800	53.51	0.09522	10.987	1.36	49.06	3.14	415.2 ± 1.1
850	42.48	0.01746	10.195	2.72	89.77	15.88	575.5 ± 0.3
875	40.32	0.01298	10.663	7.62	92.60	22.34	565.2 ± 0.2
900	39.29	0.00384	11.227	4.76	99.40	79.60	587.7 ± 0.2
925	39.53	0.00752	12.057	11.51	96.82	43.64	577.9 ± 0.1
950	39.47	0.00843	11.972	10.96	96.11	38.62	573.5 ± 0.1
975	39.73	0.00625	12.658	26.68	97.90	55.07	586.1 ± 0.2
1000	40.19	0.00669	12.794	8.18	97.62	52.02	590.5 ± 0.1
1050	39.62	0.00540	12.811	17.12	98.55	64.49	588.1 ± 0.2
1100	37.87	0.00311	10.807	1.51	99.85	94.50	571.5 ± 0.3
Fusion	39.70	0.00498	11.551	4.57	98.62	63.09	589.1 ± 0.1
Total	45.13	0.02674	12.248	100.00	94.07	49.55	576.9 ± 0.3
Total without 600–875 °C and 1100 °C-fusion				79.21			584.2 ± 0.2
Sample 9: Muscovite from garnet kyanite schists within the Meatiq J = 0.009685							
500	42.22	0.01888	0.041	1.67	86.78	0.06	540.3 ± 0.2
550	41.72	0.00127	0.042	2.30	99.09	0.90	599.3 ± 0.3
580	41.47	0.00177	0.024	3.84	98.73	0.37	594.3 ± 0.3
610	40.95	0.00062	0.048	2.91	99.55	2.12	592.1 ± 0.2
640	40.89	0.00031	0.048	3.81	99.77	4.27	592.5 ± 0.3
670	40.68	0.00130	0.029	5.86	99.04	0.60	586.2 ± 0.1
700	40.31	0.00139	0.024	10.78	98.97	0.47	581.3 ± 0.2
740	40.18	0.00088	0.016	16.79	99.35	0.50	581.6 ± 0.2
780	40.16	0.00090	0.044	15.61	99.33	1.32	581.3 ± 0.2
820	40.31	0.00157	0.032	10.66	98.84	0.55	580.6 ± 0.2
860	40.34	0.00089	0.020	11.41	99.34	0.61	583.6 ± 0.3
900	40.24	0.00091	0.043	10.08	99.33	1.29	582.3 ± 0.2
Fusion	40.57	0.00090	0.091	4.28	99.35	2.75	586.5 ± 0.1
Total	40.44	0.00135	0.034	100.00	99.01	1.01	583.1 ± 0.2
Total without 500–640 °C				85.48			582.3 ± 0.2

[a] Measured; corrected for post-irradiation decay of ^{37}Ar (35.1 day 1/2-life) + $[^{40}Ar_{tot} - (^{36}Ar_{atmos.})\ (295.5)]/^{40}Ar_{tot}$.
[b] Calculated using correction factors of Dalrymple et al. (1981); two sigma, intralaboratory errors.

660 Ma granitoids from the Meatiq (Loizenbauer et al., 2001) and the Sibai (Bregar, 1996; Fritz et al., 2000). Similar to Meatiq, the granitoids in the Hafafit intruded the enveloping high grade gneisses (Kröner et al., 1994). Apparent ages from the optically unzoned amphiboles from Hafafit (samples 7, 8) display relatively little variation within the sample and gave not rigorously defined plateau ages of 586 and 584 Ma (Fig. 6) which are very similar to those from Meatiq. The data are interpreted to data cooling below 500 °C associated with exhumation of Hafafit along localised NE-trending extensional faults (Fritz et al., 1996).

4.5. Hornblende from the Sibai dome

By contrast to Meatiq and Hafafit, Sibai constitutes predominantly juvenile magmatic rocks. Two hornblende concentrates have been prepared (Fig. 6). Sample 6 was extracted from hornblende rich portions of the Abu Markhat gneiss (Fig. 4) that intruded at ~645 Ma (Bregar, 1996) and has been later incorporated into extension tectonics (Bregar et al., 1996). We interpret the 623 Ma age to closely date cooling below 500 °C, although the plateau age is not rigorously defined. Sample 5 was taken from a foliated amphibolite lens which

represents one of rare occurrences of pre-intrusive basement (>660 Ma) in Sibai (Fig. 4). Those lenses occur in the vertically foliated and NW–SE stretched Central Gneisses which gave crystallisation ages of ~660 Ma. At the sample locality, both Central Gneisses and amphibolite lenses occur as schollen within a younger intrusion, which is part of a group of highly differentiated post-tectonic granitoids that intruded after 645 Ma. Thus the well defined plateau age of 606 Ma may reflect: (1) regional cooling in the course of denudation of Sibai; or (2) cooling after advective heating by granitoid emplacement. We emphasize that Sibai cooled below relevant blocking temperatures at least 20 Ma earlier then the Meatiq and Hafafit core complexes.

5. Interpretation

$^{40}Ar/^{39}Ar$ data presented in this study are interpreted to reflect cooling below relevant respective blocking temperatures in the course of late Neoproterozoic extension and exhumation of core complexes. Regional cooling pattern within the Central Eastern Desert includes two age groups (Figs. 7 and 8). Cooling ages from the Meatiq (mean of 4 hornblende ages 582 Ma, inter-laboratory error ~7.5 Ma) and Hafafit Core Complexes (mean of 2 hornblende ages 585 Ma, inter-laboratory error ~8 Ma) cluster around 580 Ma; those from the Sibai gave ages of 606 and 623 Ma (mean of 2 hornblende ages 615 Ma, inter-laboratory error ~7.6 Ma). Also the ages of earliest extension-related plutons is different within the three domes with ages clustering around 620 Ma in Meatiq and Hafafit and ages around 650 Ma in Sibai.

In Meatiq $^{40}Ar/^{39}Ar$ ages of both white mica and hornblende are close to the 585 Ma intrusion ages of youngest granitoid rocks and close to the ~590 Ma ages interpreted to date activity of shear zones that accommodated exhumation of the domes. This reflects rapid exhumation coevally with extension tectonics. Somewhat earlier to this upper crustal level deformation, extension started at middle crustal levels (~12 km) already around 614 Ma as indicated by emplacement dynamics of the Abu Ziran Granitoid. The combined *P–T*-deformation-time path drawn in Fig. 3 displays relations between tectonic and magmatic events in Meatiq. Rocks from the Meatiq core complex suffered a clockwise *P–T* path which contrasts the anticlockwise path obtained from the Pan-African Nappe Complex. Both structural unit cooled isobarically at ~620 Ma in 12 km depth and then experienced almost isothermal decompression due to tectonic exhumation.

In contrast to Meatiq and Hafafit, the two hornblende cooling ages of 623 and 602 Ma from the Sibai core complex are distinctly older. In Sibai, extension started already at ~660 Ma, when granitoids of the

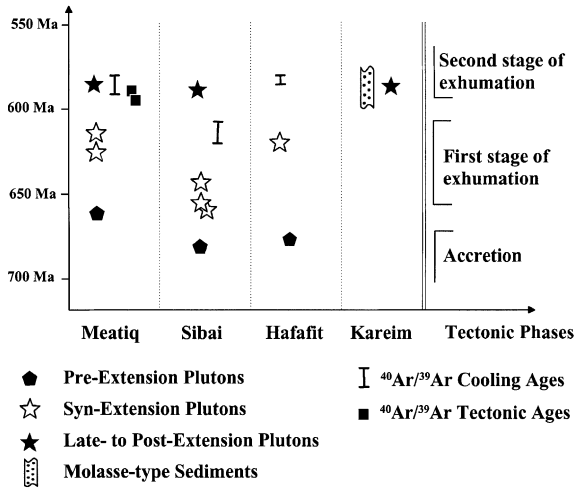

Fig. 7. Chronology of accretionary, extension and late- to post-tectonic plutonic events in the Central Eastern Desert of Egypt (Data compiled from Stern et al., 1984; Stern and Hedge, 1985; Hassan and Hashad, 1990; Kröner, 1985; Kröner et al., 1992, 1994; Stern, 1994; Abdelsalam and Stern, 1996; Blasband et al., 2000; Loizenbauer et al., 2001; Bregar et al., in press). Accretionary stage plutons include calc-alkaline bodies of El Shus Gneiss type (Sibai: Fig. 4); first extensional stage plutons include NW–SE stretched Central Gnesses at Sibai and the Abu Ziran granitoid at Meatiq (Figs. 2 and 4); late to post tectonic plutons include undeformed alkaline bodies of Arieki type (Meatiq: Fig. 2) and Atawi type (Sibai: Fig. 4). Also plotted are new $^{40}Ar/^{39}Ar$ cooling ages, $^{40}Ar/^{39}Ar$ ages that date activity of strike-slip and normal faulting in the Meatiq (Data from Fritz et al. (1996)) and reference age of sedimentation in the Kareim Basin (Data from Willis et al. (1988)).

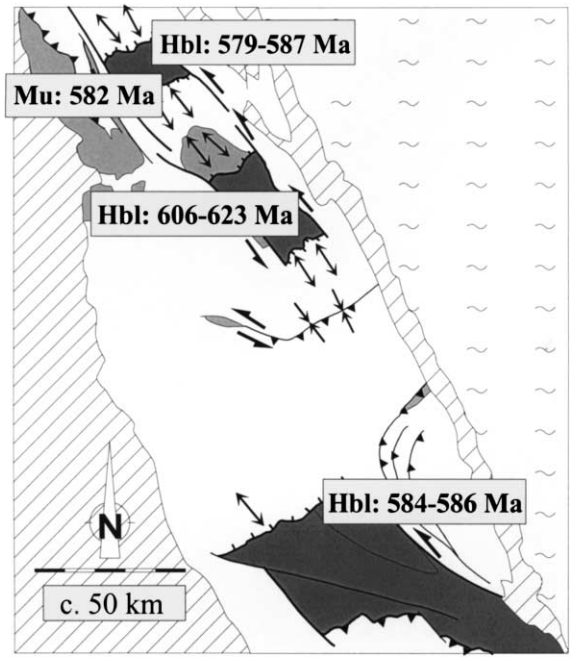

Fig. 8. Spatial variation of $^{40}Ar/^{39}Ar$ cooling ages within the Central Eastern Desert of Egypt. Hbl: hornblende; Mu: muscovite. Legend as in Fig. 1.

Central Gneisses have been intruded and stretched in NW–SE direction. No major exhumation necessarily

accompanied extension because horizontal convergence was largely balanced by NW–SE directed extension. Subsequently, upward magma migration of ~650 Ma plutons (Gebel Sibai and Gebel Markhat) was accompanied by moderated vertical mass flow and deposition of early Kareim molasse sediments in rim synclines. A second phase of rapid, tectonically-induced extension and major exhumation around 585 Ma is suggested by a line of arguments which include: (1) rapid sediment accumulation in late stage evolution of the Kareim basin; and, (2) emplacement of late- to post-tectonic granitoids coeval with molasses sedimentation.

Two scenarios may explain the variation of cooling ages within single domes in the Eastern Desert: (1) the Sibai core complex may have cooled and exhumed earlier, thereby carrying rocks below retention temperatures of Ar in hornblende. During a second stage, major exhumation associated with cooling occurred in the northerly adjacent Meatiq and the southerly Haffafit domes and, to a minor extend, Sibai. We suggest that early exhumation was a slow, magmatically induced process, whereas late stage exhumation was rapid and tectonically induced by strike-slip and normal-faults (Fig. 9). (2) Another possibility is that all three domes started to cool simultaneously during an en-block exhumation. This would imply that rocks from the Sibai crossed the 500 °C palaeo-isotherm (relevant blocking temperature for the $^{40}Ar/^{39}Ar$ hornblende system) much earlier (latest 600 Ma) and hence have been exhumed from shallower crustal levels. Continuous exhumation exposed rocks from the Meatiq and Hafafit core complexes to relevant blocking temperatures at ~580 Ma. This scenario would imply extremely low exhumation rates in early phases that likely increased with time.

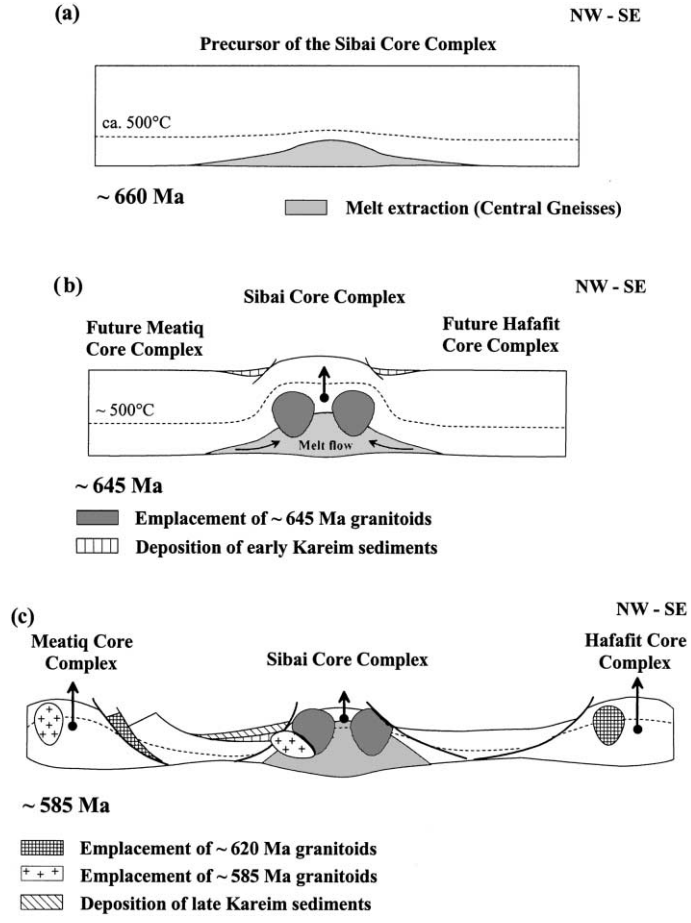

Fig. 9. Schematic model of progressively evolving extension and exhumation in the Central Eastern Desert of Egypt. (a) Extension initiated within the precursor of the Sibai Core Complex by extraction of melt at ~660 Ma when the crust-contaminated Central Gneisses (Bregar et al., in press) had been emplaced. (b) Gebel Sibai and Gebel Markhat granitoids intruded at ~645 Ma. Buoyant uprise of magma caused a rise in palaeo-isotherms and early deposition of Kareim sediments within rim synforms. Minor rock exhumation and cooling in Sibai is indicated by the black arrow. (c) Major extension associated with regional cooling at ~585 Ma exposed the Meatiq and Hafafit core complexes. The tectonically induced phase of exhumation triggered coarse-grained alluvial fan deposits in the Kareim basin north of Sibai. South to Sibai, no equivalent molasse basin is preserved due to younger tectonic activity in the Wadi Mubarak zone (E–W striking domain south of Sibai; see Fig. 1). The ~585 Ma plutons intruded the Kareim sediments and cores of Meatiq and Hafafit and terminate tectonic activity. In the course of exhumation (indicated by the black arrows) rocks from Meatiq and Hafafit have cooled below Ar retention temperatures for hornblende (~550 °C), whereas rocks above the 550 °C palaeo-isotherm had been exhumed in Sibai.

Common feature of both scenarios is that the exhumation process was slow covering a time span of 20–40 Ma. Slow, magmatically-induced exhumation at the beginning of exhumation was followed by rapid, tectonically induced exhumation at the end of the Neoproterozoic extensional history of the Nubian Shield in the Eastern Desert of Egypt.

It is worth noticing that almost all $^{40}Ar/^{39}Ar$ hornblende spectra show young ages around 400 Ma in low temperature incremental heating steps (Fig. 6). This may be explained by minor loss of radiogenic argon during a Palaeozoic thermal event and fits nicely the Fission Track (FT) data presented by Kohn et al., 1992) and Bojar et al., 2001). Based on FT ages from zircon and sphene derived from the study area, the authors argue for a Late Devonian–Early Carboniferous thermal event in the Central Eastern Desert related to intraplate tectonics (Kohn et al., 1992; Bojar et al., 2001).

6. Discussion

Exhumation of core complexes had been a substantially debated topic within the scientific community in recent years. Despite the existence of several models most authors outlined the importance of thickened crust by earlier plate convergence (Dewey, 1988; Lister and Davis, 1989; England and Houseman, 1989). These authors argue for a tectonically controlled-process (such as orogenic collapse) where exhumation was initiated when lateral buoyancy forces exceeded horizontal driving forces. This gives rise to rapid exhumation with similar cooling ages throughout the orogen and *P–T* loops that include isothermal decompression. This scenario had been suggested by Blasband et al. (2000) for the Late Neoproterozoic history in Sinai. We favour another mechanism driving exhumation in the Central Eastern Desert. In our opinion, exhumation was a long-term process that covered a time span of tens of millions of years, continuously accompanied by magmatic activity. It is important to note that the overall tectonic regime was convergent as seen by continuous shortening within foreland tectonic units.

Continuous magmatic activity together with strike-slip tectonics is typical for obliquely convergent island arc settings, ancient as well as modern (Barnes et al., 1998; Saint Blanquat et al., 1998). During oblique island arc convergence, plate motion released a partitioned deformation including sinistral strike-slip shearing and a component of orogen-parallel extension including NW–SE oriented stretching faults and NE–SW oriented normal faults. These were localised within the Najd strike-slip system where large volumes of melts had been continuously expelled (Fritz et al., 1996). We argue for a combined transpression–extrusion model (Teyssier and Tikoff, 1999) where bulk convergence is balanced by both, vertical thickening and horizontal NW–SE directed extension. The amount of vertical thickening may easily be compensated by stretch parallel to the Najd Fault System thereby triggering extension tectonics without significantly increasing the potential energy in the orogen. In our model, the ongoing convergence assists orogen-parallel extension and exhumation of core complexes. This explains the long-term process and continuous, slow exhumation. No major crustal thickening is required as convergence is continuously balanced by lateral extrusion.

We assign early exhumation of core complexes in the Central Eastern Desert as magma facilitated deformation. However, the question arises whether there is a tectonically-controlled magmatism or, vice versa, a magmatically controlled tectonism. Interference of both processes is evident in the Meatiq and Sibai core complexes as well as in the evolution of the Kareim sedimentary basin. Transpression–extrusion kinematics implies a component of horizontal shortening and vertical motion of particles following the flow line pattern (Robin and Cruden, 1994). In addition the orthogonal component of transpression during oblique plate motion imposes overpressuring that increases with the square of depth (Saint Blanquat et al., 1998). This pronounced vertical component of overpressuring is most effective in lower crustal levels and, when combined with body forces (buoyancy), effectively moves granitic melts upwards in the crust. In transpressional regimes this process creates vertically foliated and granitoids and, when combined with lateral extrusion horizontally stretched granitoids as in the case of the Central Gneisses in the Sibai. Granitoids may also intrude in regions of maximum horizontal stretching as suggested for the Abu Ziran granitoid (Fritz and Puhl, 1996). For both examples, magma emplacement is product of tectonism.

As soon as magma migrates upwards it may induce exhumation tectonics in two ways: (1) upward magma flow may be balanced by downward movement of colder and denser material inducing relative vertical mass flow. Upward motion of the Abu Sibai granitoids and early subsidence in the Kareim basin is one of those examples; and (2) even more important, magmatic activity thermally weakens the crust to facilitate extension by change in crustal rheology. We consider magmatism and shear zone activity as auto-catalytic long-terms processes that can give rise to the formation of core complexes without significant crustal thickening, and without creating significant potential energy.

Acknowledgements

We wish to thank all members of the project "Geodynamics of Pan African orogenesis in NE African" as well as participants of the 18th Colloquium on African

Geology for fruitful and ongoing discussion. An earlier version of the paper was significantly improved by Mohamed G. Abdelsalam (Dallas) and Franz Neubauer (Salzburg). Editorial handling and helpful suggestions by Peter Bowden (St. Etienne) are greatfully acknowledged. The presented work was financially supported by the Austrian Science Foundation (FWF), project P09703-Geo.

References

Abdelsalam, M.G., Stern, R.J., 1996. Sutures and shear zones in the Arabian Nubian Shield. Journal of African Earth Sciences 31, 289–310.

Barnes, P.M., Lé Pinay (de), B.M., Collot, J.-Y., Delteil, J., Audru, J.-Ch., 1998. Strain partitioning in the transition area between oblique subduction and continental collision, Hikurangi margin, New Zealand. Tectonics 17, 534–557.

Baldwin, S.L., Harrison, T.M., Gerald, J.D., 1990. Diffusion of 40Ar in metamorphic hornblende. Contributions Mineralogy Petrology 105, 691–703.

Blanckenburg, F., Villa, I.M., Baur, H., Morteani, G., Steiger, R.H., 1989. Time calibration of a *P–T* path from the western Tauern Window, eastern Alps: The problem of closure temperatures. Contribution to Mineralogy and Petrology 101, 1–11.

Blasband, B., White, S., Brooijmans, P., De Boorder, H., Visser, W., 2000. Late Proterozoic extensional collapse in the Arabian–Nubian Shield. Journal of the Geological Society, London 157, 615–628.

Bojar, A.-V., Fritz, H., Kargl, S., Unzog, W., 2001. Phanerozoic tectonothermal history of the Arabian–Nubian Shield in the Eastern Desert of Egypt evidence from fission track and paleostress data. Journal of African Earth Sciences 34, pp. 201–212.

Bregar, M., 1996. Exhumation history of the Gebel Sibai Dome (Eastern Desert of Egypt): Constraints from evolution of low-angle normal faults and corresponding footwall units. M.Sc. Thesis, University of Graz.

Bregar, M., Fritz, H., Unzog, W., 1996. Structural evolution of low-angle normal faults SE of the Gebel El Sibai Crystalline Dome; Eastern Desert, Egypt: Evidence from paleopiezometry and vorticity analysis. Zentralblatt Geologie Paläontologie 3/4, 243–256.

Bregar, M., Bauernhofer, A., Pelz, K., Kloetzli, U., Fritz, H., Neumayr, P., in press. A late Neoproterozoic magmatic core complex in the Eastern desert of Egypt: Emplacement of granitoids in a wrench-tectonic setting.

Burke, K., Sengör, C., 1986. Tectonic escape in the evolution of the continental crust. In: Barazangi, M. (Ed.), Reflection Seismology the continental crust, vol. 14, pp. 41–53.

Cliff, R.A., 1985. Isotopic dating in metamorphic belts. Journal Geological Society London 142, 97–110.

Dallmeyer, R.D., Takasu, A., 1992. $^{40}Ar/^{39}Ar$ of detrital muscovite and whole rock slate/phyllite, Narragansett Basin, RI-MA, USA: implications for rejuvenation during very low-grade metamorphism. Contributions to Mineralogy and Petrology 110, 515–527.

Dallmeyer, R.D., Neubauer, F., Höck, V., 1992. Chronology of late Paleozoic tectonothermal activity in the southeastern Bohemian Massif, Austria (Moldanubian and Moravo–Silesian Zone): $^{40}Ar/^{39}Ar$ mineral age controls. Tectonophysics 210, 135–153.

Dalrymple, G.B., Alexander, E.C., Lanphere, M.A., Kraker, G.P., 1981. Irradiation of samples for 40Ar/39Ar dating using the Geological Survey TRIGA reactor. US Geological Survey Professional Paper 1176, 1–55.

Davis, J.H., Blanckenburg, F., 1995. Slab breakoff: A model of lithosphere detachment and its test in the magmatism and deformation of collisional orogens. Earth and Planetary Science Letters 129, 85–102.

Dewey, J.F., 1988. Extensional collapse of orogens. Tectonics 7, 1123–1139.

Dodson, M.H., 1973. Closure temperature in cooling geochronological and petrological systems. Contributions Mineralogy Petrology 40, 259–274.

El Gaby, S., List, F.K., Tehrani, R., 1990. The basement complex of the Eastern Desert and Sinai. In: Rushdi, S. (Ed.), The Geology of Egypt. Balkema, Rotterdam, pp. 175–184.

England, P.C., Houseman, G.A., 1989. Extension during continental convergence, with application to the Tibetan plateau. Journal of Geophysical Research 94, 17561–17579.

England, P.C., Thompson, A.B., 1984. Pressure-temperature-time paths of regional metamorphism, I, Heat transfer during the evolution of regions of thickened continental crust. Journal of Petrology 25, 894–928.

England, P.C., Molnar, P., 1990. Surface uplift, uplift of rocks and exhumation of rocks. Geology 18, 1173–1177.

Fritz, H., Wallbrecher, E., Khudeir, A.A., Abu El Ela, F., Dallmeyer, D.R., 1996. Formation of Neoproterozoic metamorphic core complexes during oblique convergence (Eastern Desert, Egypt). Journal of African Earth Sciences 23, 311–323.

Fritz, H., Puhl, J., 1996. Granitoid emplacement in a shear-extensional setting: A semiquantitative approach from physical parameters (Eastern Desert, Egypt). Zentralblatt Geologie Paläontologie, 257–276.

Fritz, H., Messner, M., 1999. Intramontane basin formation during oblique convergence in the Eastern desert of Egypt: magmatically versus tectonically induced subsidence. Tectonophysics 315, 145–162.

Fritz, H., Wallbrecher, E., Loizenbauer, J., Hoinkes, G., Dallmeyer, R.D., Khudier, A., 2000. Crustal evolution during oblique convergence, transpression and extrusion within the central Eastern Desert of Egypt: a slow velocity process. Journal of African Earth Sciences 33, 33–34.

Fowler, T.J., Osman, A.F., 2001. Gneiss-cored interference dome associated with two phases of late Pan-African thrusting in the central Eastern Desert, Egypt. Precambrian Research 108, 7–43.

Garfunkel, Z., 1988. Relation between continental rifting and uplift: evidence from the Suez rift and the northern Red Sea. Tectonophysics 150, 33–49.

Gass, I.G., 1982. Upper Proterozoic Pan African calcalkaline magmatism in northeastern Africa and Arabia. In: Thorpe, R.S. (Ed.), Andesites. Wiley, New York, pp. 591–609.

Greiling, R.O., Abdeen, M.M., Dardir, A.A., El Akhal, H., El Ramly, M.F., Kamal El-Din, G.M., Osman, A.F., Rashwan, A.A., Rice, A.H.N., Sadek, M.F., 1994. A structural synthesis of the Proterozoic Arabian–Nubian Shield in Egypt. Geologische Rundschau 83, 484–501.

Grothaus, B.D., Eppler, D., Ehrlich, R., 1979. Depositional environment and structural implications of the Hammamat Formation, Egypt. Annual Geological Survey Egypt 9, 564–590.

Harrison, T.M., 1981. Diffusion of ^{40}Ar in hornblende. Contribution Mineralogy Petrology 78, 324–331.

Hames, W.E., Bowring, S.A., 1994. An empirical evaluation of the argon diffusion geometry in muscovite. Earth and Planetary Science Letters 124, 161–167.

Hassan, M.A., Hashad, A.H., 1990. Precambrian of Egypt. In: Rushdi, S. (Ed.), The Geology of Egypt. Balkema, Rotterdam, pp. 201–248.

Houseman, G.A., McKenzie, D.P., Molnar, P., 1981. Convective instability of a thickened boundary layer and its relevance for the thermal evolution of continental convergence belts. Journal of Geophysical Research 86, 6115–6132.

Kamal El Din, G.M., 1993. Geochemistry and tectonic significance of the Pan-African El Sibai window, Central Eastern Desert, Egypt.

Scientific Series of the International Bureau/Forschungszentrum Jüllich 19, 154.

Kamal El Din, G.M., 2000. Late-Pan-African extension/compression interplay and the structural evolution of the molasse-type Hammamat basin: an example from the Wadi Kariem Basin, Eastern Desert, Egypt. Journal of African Earth Sciences, Special Abstract Issue 30/4A, 44.

Khudeir, A.A., El-Gaby, S., Kamal El-Din, G.M., Asran, A.M.H., Greiling, R.O., 1995. The pre-Panafrican deformed granite cycle of the Gabal El-Sibai swell, Eastern Desert, Egypt. Journal African Earth Sciences 21 (3), 395–406.

Kohn, B.P., Eyal, M., Feinstein, S., 1992. A major Late Devonian-Early Carboniferous (Hercynian) thermotectonic event at the NW margin of the Arabian–Nubian shield. Evidence from zircon fission track dating.. Tectonics 11/5, 1018–1027.

Kröner, A., 1985. Ophiolites and the evolution of tectonic boundaries in the late Proterozoic Arabian–Nubian Shield of Northeast Africa and Arabia. Precambrian Research 27, 235–257.

Kröner, A., Todt, W., Hussein, I.M., Mansour, M., Rashwan, A.A., 1992. Dating of late Proterozoic ophiolites in Egypt and the Sudan using the single grain zircon evaporation technique. Precambrian Research 59, 15–32.

Kröner, A., Krüger, J., Rashwan, A.A., 1994. Age and tectonic setting of granitoid gneisses in the Eastern Desert of Egypt and south–west Sinai. Geologische Rundschau 83, 502–513.

Lister, G.S., Davis, G.A., 1989. The origin of metamorphic core complexes and detachment faults during continental extension in the northern Colorado River region, USA. Journal of Structural Geology 11, 65–94.

Loizenbauer, J., 1998. Exhumation history of the Meatiq Metamorphic Core Complex and gold mineralisation during Pan-African Orogeny in the Eastern Desert, Egypt-Evidence from Fluid Inclusion studies and Structural Geology. Ph.D. Thesis, University of Graz, Austria.

Loizenbauer, J., Wallbrecher, E., Fritz, H., Neumayr, P., Khudeir, A.A., Kloetzli, U., 2001. Structural geology, single zircon ages and fluid inclusion studies of the Meatiq metamorphic core complex: Implications for Neoproterozoic tectonics in the Eastern Desert of Egypt. Precambrian Research 110, 357–383.

McDougall, I., Harrison, T.M., 1999. Geochronology and Thermochronology by the $^{40}Ar/^{39}Ar$ Method, second ed. Oxford University Press, Oxford, pp. 269.

Messner, M., Fritz, H., Pelz, K., Unzog, W., 1996. Beckenbildung in verschiedenen tektonischen Settings: Struktureller Rahmen und Abbildung der Tektonik in der Sedimentation. In: Symposium Tektonik, Strukturgeologie, Kristallingeologie, vol. 6. Facultas Verlag, Salzburg, pp. 275–278.

Neubauer, F., Genser, J., Kurz, W., Wang, X., 1999. Exhumation of the Tauern window, Eastern Alps. Physics and Chemistry of the Earth 24, 675–680.

Neumayr, P., Hoinkes, G., Puhl, J., 1995. Constraints on the P–T–t evolution of a polymetamorphic Panafrican basement dome in the Central Eastern Desert (Egypt). Terra Abstracts 7, 316.

Neumayr, P., Mogessie, A., Hoinkes, G., Puhl, J., 1996. Geological setting of the Meatiq metamorphic core complex in the Eastern Desert of Egypt based on amphibolite geochemistry. Journal African Earth Sciences 23, 331–345.

Neumayr, P., Hoinkes, G., Puhl, J., Mogessie, A., Khudeir, A.A., 1998. The Meatiq dome (Eastern Desert, Egypt) a Precambrian metamorphic core complex: petrological and geological evidence. Journal of Metamorphic Geology 16, 259–279.

Oldow, J.S., Bally, A.W., Lallemant, H.G.A., 1990. Transpression, orogenic float, and lithospheric balance. Geology 18, 991–994.

Omar, G.I., Steckler, M.S., Buck, W.R., Kohn, B.P., 1989. Fission track analysis of basement apatites at the western margin of the Gulf of Suez rift Evidence for synchronicity of uplift and subsidence. Earth and Planetary Science Letters 94, 316–329.

Onstott, T.C., Peacock, M.W., 1987. Argon retentivity of hornblende. A field experiment in a slow cooling metamorphic terrain. Geochimica and Cosmochimica Acta 51, 2891–2903.

Pelz, K., 1996. Exhumation history of the Sibai Dome, Central Eastern Desert, Egypt Constraints from the kinematic evolution of the southwestern shear zone. M.Sc. Thesis, University of Graz, Austria.

Platt, J.P., England, P.C., 1994. Convective removal of lithosphere beneath mountain belts: Thermal and mechanical consequences. American Journal of Science 294, 307–336.

Postma, G., 1990. Depositional architecture and facies of river and fan deltas a synthesis. In: Collela, A., Prior, D.B. (Eds.), Coarse-Grained Deltas. Blackwell, Oxford, pp. 13–28.

Puhl, J., 1997. Die Petrogenese des Meatiq-Kristallindomes, Östliche Zentralarabische Wüste, Ägypten. M.Sc. Thesis, University of Graz, Austria.

Rashwan, A.A., 1991. Petrography, geochemistry and petrogenesis of the Migif–Hafafit Mine area, Egypt. Scientific Series of the International Bureau/Forschungszentrum Jülich 5, 359.

Rice, A.H.N, Sadek, M.-F., Rashwan, A.A., 1993. Igneous and structural relations in the Pan-African Hammamat Group Igla Basin Egypt. In: Thorweihe, U., Schandelmeier, H. (Eds.), Geoscientific Research in Northeast Africa. Balkema, Rotterdam, pp. 35–39.

Ries, A.C., Shackleton, R.M., Graham, R.H., Fitches, W.R., 1983. Pan-African structures, ophiolites and melanges in the Eastern Desert of Egypt a traverse at 26°N. Journal of the Geological Society, London 140, 75–95.

Robbins, C.S., 1972. Radiogenic argon diffusion in muscovite under hydrothermal conditions. MSc Thesis, Brown University, Providence, Rhode Island, USA.

Robin, P.-Y.F., Cruden, A.R., 1994. Strain and vorticity patterns in ideal transpression zones. Journal of Structural Geology 16, 447–466.

Saint Blanquat (de), M., Tikoff, B., Teyssier, Ch., Vigneresse, J.L., 1998. Transpressional kinematics and magmatic arcs. In: Holdsworth, R.E., Strachan, R.A., Dewey, J.F. (Eds.), Continental Transpression and Transtension Tectonics, vol. 135. Geological Society of London, Special Publications, pp. 327–340.

Samson, S.D., Alexander Jr., E.C., 1987. Calibration of the interlaboratory $^{40}Ar/^{39}Ar$ dating standart Mmhb 1. Chemical Geology 66, 27–34.

Sandiford, M., Powell, R., 1990. Some isostatic and thermal consequences of the vertical strain geometry in convergent orogens. Earth and Planetary Science Letters 98, 145–165.

Sandiford, M., Martin, N., Zhou, S., Fraser, G., 1991. Mechanical consequences of granite emplacement during high-*T*, low-*P* metamorphism and the origin of anticlockwise *PT* paths. Earth and Planetary Science Letters 107, 164–172.

Schmidt, M.W., 1992. Amphibole composition in tonalite as a function of pressure: an experimental calibration of Al-in-hornblende barometer. Contribution Mineralogy Petrology 110, 304–310.

Steiger, R.H., Jäger, E., 1977. Subcommission on geochronology convention on the use of decay constants in geo- and cosmochronolgy. Earth and Planetary Science Letters 36, 359–362.

Stern, R., 1985. The Najd Fault System, Saudi Arabia and Egypt: A late Precambrian rift-related transform system? Tectonics 4, 497–511.

Stern, R.J., 1994. Arc Assembly and Continental Collision in the Neoproterozoic East African Orogen Implications for the Consolidation of Gondwanaland. Annual Reviews Earth and Planetary Science Letters 22, 319–351.

Stern, R.J., Gottfried, D., Hedge, C.E., 1984. Late Precambrian rifting and crustal evolution in the Northeastern Desert of Egypt. Geology 12, 168–172.

Stern, R.J., Hedge, C., 1985. Geochronologic and isotopic constraints on late Precambrian crustal evolution in the Eastern Desert of Egypt. American Journal of Science 285, 97–172.

Stuewe, K., Barr, T.D., 1998. On uplift and exhumation during convergence. Tectonics 17, 80–88.

Sturchio, N.C., Sultan, M., Batiza, R., 1983. Geology of the Meatiq Dome, Egypt: A Precambrian metamorphic core complex? Geology 11, 72–76.

Tapponier, P., Molnar, P., 1976. Slip-line field theory and large scale continental tectonics. Nature 264, 319–324.

Teyssier, Ch., Tikoff, B., Markley, M., 1995. Oblique plate motion and continental tectonics. Geology 23, 447–450.

Teyssier, Ch., Tikoff, B., 1999. Fabric stability in oblique convergence and divergence. Journal of Structural Geology 21, 969–974.

Tikoff, B., Teyssier, Ch., 1994. Strain modelling of displacement-field partitioning in transpressional orogens. Journal of Structural Geology 16, 1575–1588.

Wallbrecher, E., Fritz, H., Khudeir, A.A., Farahad, F., 1993. Kinematics of Panafrican thrusting and extension in Egypt. In: Thorweihe, U., Schandelmeier, H. (Eds.), Geoscientific Research in Northeast Africa. Balkema, Rotterdam, pp. 27–30.

Warren, R.G., Ellis, D.J., 1996. Mantle underplating, granite tectonics, and metamorphic *P–T–t* paths. Geology 24, 663–666.

Weinberg, R.F., Podladchikov, Y., 1995. The rise of solid state diapirs. Journal of Structural Geology 17, 1183–1195.

Willis, K.M., Stern, R.J., Clauer, N., 1988. Age and geochemistry of late Precambrian sediments of the Hammamat series from the Northeastern Desert of Egypt. Precambrian Research 42, 173–187.